J. Fluid Mech. (2001), *vol.* 447, *pp.* 149–171.
DOI: 10.1017/S002211200100578X Printed in the United Kingdom

On the motion of multiple helical vortices

By D. H. WOOD[1] AND J. BOERSMA[2]

[1]Department of Mechanical Engineering, University of Newcastle, NSW 2308, Australia

[2]Department of Mathematics and Computing Science, Eindhoven University of Technology, 5600 MB Eindhoven, The Netherlands

(Received 4 January 2001 and in revised form 21 May 2001)

The analysis of the self-induced velocity of a single helical vortex (Boersma & Wood 1999) is extended to include equally spaced multiple vortices. This arrangement approximates the tip vortices in the far wake of multi-bladed wind turbines, propellers, or rotors in ascending, descending, or hovering flight. The problem is reduced to finding, from the Biot–Savart law, the additional velocity of a helix due to an identical helix displaced azimuthally. The resulting Biot–Savart integral is further reduced to a Mellin–Barnes integral representation which allows the asymptotic expansions to be determined for small and for large pitch. The Biot–Savart integral is also evaluated numerically for a total of two, three and four vortices over a range of pitch values. The previous finding that the self-induced velocity at small pitch is dominated by a term inversely proportional to the pitch carries over to multiple vortices. It is shown that a far wake dominated by helical tip vortices is consistent with the one-dimensional representation that leads to the Betz limit on the power output of wind turbines. The small-pitch approximation then allows the determination of the blade's bound vorticity for optimum power extraction. The present analysis is shown to give reasonable estimates for the vortex circulation in experiments using a single hovering rotor and a four-bladed propeller.

1. Introduction

The self-induced motion of an infinite helical vortex has recently been investigated in some detail. Ricca (1994) formulated the problem in two ways: first, as the limiting case of the exact solution of Hardin (1982) for the inviscid flow outside a helical line vortex (of zero thickness); secondly, using the Moore–Saffman (MS) procedure (Moore & Saffman 1972) for applying the Biot–Savart law to a vortex whose core radius is small compared to its radius of curvature. The MS procedure removes the curvature-induced singularity by use of an osculating vortex ring of the same core radius; see e.g. Saffman (1992). Ricca (1994) evaluated numerically the resulting integrals for the binormal velocity of the vortex, the most important velocity since helical vortices translate without deformation. Kuibin & Okulov (1998) determined the asymptotic expansion for the velocity at small values of the vortex pitch, p. This expansion was slightly refined by Boersma & Wood (1999, hereinafter referred to as BW) on the basis of their closed-form expression for the binormal velocity that is valid for all values of p. They also proved the close connection between the results of Ricca's (1994) two formulations.

The remarkable outcome of these investigations is that the 'remainder' term – the contribution to the self-induced velocity from the parts of the vortex that do *not* contribute to the curvature singularity – dominates the curvature term at small values of p. This is in contrast to the vortex ring, for example, whose velocity is due almost entirely to its curvature. Kuibin & Okulov (1998) and BW showed that the remainder term for a helical vortex behaves like p^{-1} as $p \downarrow 0$.

In practice, however, it is much more common that *multiple* helical vortices occur in the wakes of wind turbines, propellers, and ascending, descending, or hovering helicopters; an N-bladed rotor produces N nominally identical helical vortices, spaced $2\pi/N$ radians apart. In many cases the pitch of these tip vortices is sufficiently small for the asymptotic form of the remainder to be useful. The purpose of the present work is to extend the analysis of BW to the general problem of N equally spaced infinite helical vortices. Our major findings are that the leading p^{-1}-term found for a single vortex carries over to a term N/p for multiple vortices and the dependence on the azimuthal spacing between the vortices is of higher order.

The general problem is linear and is reduced, in the next section, to that of finding the binormal velocity induced on a helical vortex by an identical vortex that is azimuthally displaced α radians from the first vortex. The velocity is obtained directly from the Biot–Savart law, without using the MS procedure, as the displaced vortex does not introduce any further singularities. In Appendix A we demonstrate the equivalence of this formulation and the one based on Hardin's (1982) solution. The next section provides the large- and small-pitch asymptotic expansions for the integral expressing the binormal velocity. This is followed by a description of the numerical evaluation of the integral for $\alpha = \pi/2$, $2\pi/3$ and π (needed in the most common cases $N = 2$, 3, and 4), based on the treatment of BW. Then, some of the implications of the analysis for the modelling of rotor wakes are presented, followed by the conclusions.

2. Reduction of the general problem

The general problem is to determine the velocity induced by an arrangement of N identical helical vortices, spaced $2\pi/N$ radians apart. Of main interest is the binormal velocity induced at a point $\boldsymbol{X}$ on one of the helices. This velocity is given by the sum of the self-induced contribution and the contributions of the remaining $N-1$ vortices. In BW the self-induced contribution to the binormal velocity was expressed in terms of the integral $W(p)$, defined in BW (4.1) (BW before an equation number denoting a formula from Boersma & Wood 1999) by

$$W(p) = \int_0^\infty \left\{ \frac{\sin^2 t}{(p^2t^2 + \sin^2 t)^{3/2}} - \frac{1}{(p^2+1)^{3/2}} \frac{H(1/2-t)}{t} \right\} \mathrm{d}t, \tag{2.1}$$

in which $H(\cdot)$ denotes the unit step function. The remaining problem can be reduced to that of finding the binormal velocity induced by a single helical vortex $\mathscr{H}$ at the point $\boldsymbol{X}$ of an identical helix that is azimuthally displaced α radians from $\mathscr{H}$, where $0 < \alpha < 2\pi$ (actually, $\alpha = 2\pi j/N$ with $j = 1, 2, \ldots, N-1$). Let the infinite helix $\mathscr{H}$ have the parametric representation (in Cartesian coordinates)

$$\boldsymbol{X}^* = (x, y, z) = (R\cos\theta, R\sin\theta, pR\theta) \quad (-\infty < \theta < \infty) \tag{2.2}$$

where R is the radius and p is the (normalized) pitch of the helical vortex. Without loss of generality, we consider the point $\boldsymbol{X}$ displaced α radians from the point $(R, 0, 0)$

of $\mathscr{H}$. Then $\boldsymbol{X}$ has Cartesian coordinates

$$\boldsymbol{X} = (R\cos\alpha, -R\sin\alpha, 0). \tag{2.3}$$

Following Ricca (1994, equation (1.1)) the induced velocity $\boldsymbol{U} = \boldsymbol{U}(\boldsymbol{X})$ at $\boldsymbol{X}$ is given by the Biot–Savart law

$$\boldsymbol{U}(X) = \frac{\Gamma}{4\pi}\int_{\mathscr{H}} \frac{\boldsymbol{t}(\boldsymbol{X}^*)\times(\boldsymbol{X}-\boldsymbol{X}^*)}{|\boldsymbol{X}-\boldsymbol{X}^*|^3}\,\mathrm{d}s, \tag{2.4}$$

where Γ is the vortex circulation and s denotes arclength along the helix $\mathscr{H}$. The unit tangent vector $\boldsymbol{t}(\boldsymbol{X}^*)$ to $\mathscr{H}$ has Cartesian components

$$\boldsymbol{t}(\boldsymbol{X}^*) = \frac{1}{(p^2+1)^{1/2}}(-\sin\theta, \cos\theta, p), \tag{2.5}$$

while $\mathrm{d}s = (p^2+1)^{1/2}R\mathrm{d}\theta$. Take the inner product of $\boldsymbol{U}(\boldsymbol{X})$ and the binormal $\boldsymbol{b}(\boldsymbol{X})$ of the displaced helix at $\boldsymbol{X}$, given by

$$\boldsymbol{b}(\boldsymbol{X}) = \frac{p}{(p^2+1)^{1/2}}\left(-\sin\alpha, -\cos\alpha, \frac{1}{p}\right). \tag{2.6}$$

On evaluation of the vector and inner products, the required binormal velocity is found to be

$$U_b = \boldsymbol{b}(\boldsymbol{X})\cdot\boldsymbol{U}(\boldsymbol{X}) = \frac{\Gamma}{4\pi R} I_b(\alpha, p), \tag{2.7}$$

where the normalized or dimensionless binormal velocity $I_b(\alpha, p)$ is given by

$$I_b(\alpha,p) = \frac{1}{(p^2+1)^{1/2}}\int_{-\infty}^{\infty} \frac{p^2\theta\sin(\theta+\alpha) + (1-p^2)[1-\cos(\theta+\alpha)]}{[p^2\theta^2 + 2\{1-\cos(\theta+\alpha)\}]^{3/2}}\,\mathrm{d}\theta. \tag{2.8}$$

Because the helix $\mathscr{H}$ is infinite, the result (2.7) is valid at all points of the displaced helix through $\boldsymbol{X}$.

By use of

$$\frac{p^2\theta\sin(\theta+\alpha) - 2p^2[1-\cos(\theta+\alpha)]}{[p^2\theta^2 + 2\{1-\cos(\theta+\alpha)\}]^{3/2}} = -\frac{\mathrm{d}}{\mathrm{d}\theta}\left(\frac{p^2\theta}{[p^2\theta^2 + 2\{1-\cos(\theta+\alpha)\}]^{1/2}}\right)$$

in the integrand of (2.8), we express $I_b(\alpha, p)$ as

$$I_b(\alpha,p) = (p^2+1)^{1/2}W(\alpha,p) - \frac{2p}{(p^2+1)^{1/2}}, \tag{2.9}$$

where, with the substitution $\theta = 2t$,

$$W(\alpha,p) = \frac{1}{2}\int_{-\infty}^{\infty} \frac{\sin^2(t+\alpha/2)}{[p^2t^2 + \sin^2(t+\alpha/2)]^{3/2}}\,\mathrm{d}t, \quad 0<\alpha<2\pi. \tag{2.10}$$

It is believed that the integral $W(\alpha, p)$ cannot be evaluated in closed form. Therefore, in the next section we consider the asymptotics of $W(\alpha, p)$ both for small p and for large p. From (2.10) it is obvious that

$$W(\alpha,p) = W(2\pi-\alpha,p), \tag{2.11}$$

which means, for example, that the second and third vortices induce the same velocity on the first when $N = 3$. For $\alpha = 0$ the integral (2.10) becomes divergent. Thus before taking the limit of $W(\alpha, p)$ as $\alpha \downarrow 0$, one should subtract a proper singularity. At the

end of Appendix B it is shown that (see (B 32))

$$\lim_{\alpha\downarrow 0}[W(\alpha,p)+\log[2\sin(\alpha/2)](p^2+1)^{-3/2}]$$
$$=W(p)+(p^2+1)^{-3/2}[p^2-1+\log 2+\log(p^2+1)-\log p], \quad (2.12)$$

where $W(p)$ is given by (2.1). $W(p)$ can be considered as the finite part of the limit of $W(\alpha,p)$ as $\alpha\downarrow 0$.

BW also discussed in depth the relationship between the induced velocity obtained from the Biot–Savart law and that from Hardin's (1982) formulation. There is a small difference between the two results due to the requirement in the MS procedure to account for the finite size and particular structure of the vortex core, and the ignoring of those aspects by Hardin. In the present case, the velocity required is not self-induced and the two methods should give the same result. It is shown in Appendix A that the induced velocity from Hardin's (1982) solution reduces to (2.9).

3. The asymptotics of $W(\alpha,p)$

In this section we determine the asymptotic expansions of $W(\alpha,p)$ for small ($p\downarrow 0$) and large ($p\to\infty$) pitch. Both expansions are obtained from a Mellin–Barnes integral representation of $W(\alpha,p)$, as derived in Appendix B; see (B 23) and (B 24). The limit for large pitch is often called the Kelvin limit; see e.g. Ricca (1994, formula (3.20)). We will demonstrate that for this limit there is a larger difference between $W(\alpha,p)$ and $W(p)$, than there is at small pitch. On the other hand, it is shown in § 5 that the application of the analysis to the wakes of propellers, wind turbines, and ascending, descending, or hovering rotors, generally involves the small-pitch limit.

3.1. $W(\alpha,p)$ *for small pitch* ($p\downarrow 0$)

We start from the Mellin–Barnes integral representation (B 24) for $W(\alpha,p)$. The integrand in (B 24) is analytic to the left of the integration contour, except for simple poles at $z=-2k$, $k=1,2,3,\ldots$, with residues

$$\mathrm{Res}_{z=-2k}\frac{\Gamma(z/2)\Gamma(3/2-z/2)}{2\Gamma(3/2)}L^*(z)p^{-z}=(-1)^k\frac{(3/2)_k}{k!}L^*(-2k)p^{2k}, \quad (3.1)$$

where $\Gamma(\cdot)$ denotes the gamma function and Pochhammer's symbol $(3/2)_k$ is defined by

$$(3/2)_0=1, \quad (3/2)_k=\tfrac{3}{2}\cdot\tfrac{5}{2}\cdots(k+\tfrac{1}{2}) \quad \text{for} \quad k=1,2,3,\ldots.$$

Since $L^*(0)=0$ from (B 22), the singularity of the integrand at $z=0$ is removable. By closing the contour in (B 24) to the left, we are led to the representation of $W(\alpha,p)$ by the residue series

$$W(\alpha,p)\sim\frac{1}{p}-\log[2\sin(\alpha/2)]\,(p^2+1)^{-3/2}$$
$$+\sum_{k=1}^{\infty}(-1)^k\frac{(3/2)_k}{k!}L^*(-2k)p^{2k} \quad (p\downarrow 0). \quad (3.2)$$

This result forms the complete asymptotic expansion of $W(\alpha,p)$ for small p.

We now introduce the generalized Clausen function of odd order, $\mathrm{Cl}_{2k+1}(\theta)$, defined by

$$\mathrm{Cl}_{2k+1}(\theta) = \sum_{n=1}^{\infty} \frac{\cos(n\theta)}{n^{2k+1}}; \tag{3.3}$$

see Lewin (1981, p. 191). This function is employed in the evaluation of $L^*(-2k)$ for $k = 1, 2, 3$. Starting from (B 22) we have

$$\begin{aligned} L^*(-2) &= \sum_{n=1}^{\infty} \left[\frac{\Gamma(n+3/2)}{\Gamma(n-1/2)} \frac{1}{n^3} - \frac{1}{n} \right] \cos(n\alpha) = \sum_{n=1}^{\infty} \left[\frac{n^2 - 1/4}{n^3} - \frac{1}{n} \right] \cos(n\alpha) \\ &= -\frac{1}{4} \sum_{n=1}^{\infty} \frac{\cos(n\alpha)}{n^3} = -\tfrac{1}{4}\mathrm{Cl}_3(\alpha), \end{aligned}$$

$$L^*(-4) = \sum_{n=1}^{\infty} \left[\frac{(n^2 - 1/4)(n^2 - 9/4)}{n^5} - \frac{1}{n} \right] \cos(n\alpha) = -\tfrac{5}{2}\mathrm{Cl}_3(\alpha) + \tfrac{9}{16}\mathrm{Cl}_5(\alpha),$$

$$\begin{aligned} L^*(-6) &= \sum_{n=1}^{\infty} \left[\frac{(n^2 - 1/4)(n^2 - 9/4)(n^2 - 25/4)}{n^7} - \frac{1}{n} \right] \cos(n\alpha) \\ &= -\tfrac{35}{4}\mathrm{Cl}_3(\alpha) + \tfrac{259}{16}\mathrm{Cl}_5(\alpha) - \tfrac{225}{64}\mathrm{Cl}_7(\alpha). \end{aligned}$$

By use of these values in (3.2) we obtain the small-p expansion

$$\begin{aligned} W(\alpha, p) = {} & p^{-1} - \log[2\sin(\alpha/2)](p^2+1)^{-3/2} + \tfrac{3}{8}\mathrm{Cl}_3(\alpha)p^2 \\ & + \tfrac{15}{8}[-\tfrac{5}{2}\mathrm{Cl}_3(\alpha) + \tfrac{9}{16}\mathrm{Cl}_5(\alpha)]p^4 \\ & - \tfrac{35}{16}[-\tfrac{35}{4}\mathrm{Cl}_3(\alpha) + \tfrac{259}{16}\mathrm{Cl}_5(\alpha) - \tfrac{225}{64}\mathrm{Cl}_7(\alpha)]p^6 + O(p^8) \ (p \downarrow 0). \end{aligned} \tag{3.4}$$

We note the following special values of $\mathrm{Cl}_{2k+1}(\theta)$:

$$\mathrm{Cl}_{2k+1}(0) = \zeta(2k+1), \quad \mathrm{Cl}_{2k+1}(\pi) = -(1 - 2^{-2k})\zeta(2k+1), \tag{3.5}$$

where $\zeta(\cdot)$ denotes the Riemann zeta function. For later use, and in view of (2.11), we also note from Lewin (1981, p. 198) that

$$\left.\begin{aligned} \mathrm{Cl}_{2k+1}(\pi/2) = \mathrm{Cl}_{2k+1}(3\pi/2) &= -2^{-2k-1}(1 - 2^{-2k})\zeta(2k+1), \\ \mathrm{Cl}_{2k+1}(\pi/3) = \mathrm{Cl}_{2k+1}(5\pi/3) &= \tfrac{1}{2}(1 - 2^{-2k})(1 - 3^{-2k})\zeta(2k+1), \\ \mathrm{Cl}_{2k+1}(2\pi/3) = \mathrm{Cl}_{2k+1}(4\pi/3) &= -\tfrac{1}{2}(1 - 3^{-2k})\zeta(2k+1). \end{aligned}\right\} \tag{3.6}$$

The values in (3.5) and (3.6) are sufficient to evaluate (3.4) for 2-, 3- and 4-bladed rotors. In general, the following relation from Lewin (1981, p. 198) may be useful for an N-bladed rotor for which the vortices are spaced $2\pi/N$ apart:

$$\sum_{j=0}^{N-1} \mathrm{Cl}_{2k+1}\left(\frac{2\pi j}{N}\right) = \frac{1}{N^{2k}}\mathrm{Cl}_{2k+1}(0) = \frac{1}{N^{2k}}\zeta(2k+1), \tag{3.7}$$

showing that there can be significant advantages in considering the effects of the N vortices together.

3.2. $W(\alpha, p)$ *for large pitch* $(p \to \infty)$

For this case, it is easier to start from the Mellin–Barnes integral representation (B 23) rather than (B 24). The integrand in (B 23) is analytic to the right of the integration contour, except for double poles at $z = 2k + 1$, $k = 1, 2, 3, \ldots$. By closing the contour to the right, we are led to the representation of $W(\alpha, p)$ by the residue series

$$W(\alpha, p) \sim \frac{1}{p} - \sum_{k=1}^{\infty} \mathrm{Res}_{z=2k+1} \left[\frac{\Gamma(z/2)\Gamma(3/2 - z/2)}{2\,\Gamma(3/2)} L(z)\, p^{-z} \right] \quad (p \to \infty). \tag{3.8}$$

This result forms the complete asymptotic expansion of $W(\alpha, p)$ for large p. It does not appear possible to obtain simple, general, closed-form expressions for the residues. Instead, we consider only the cases $k = 1$ and $k = 2$, corresponding to the residues at $z = 3$ and $z = 5$.

(i) Around $z = 3$ we have the Laurent expansions

$$\frac{\Gamma(z/2)\Gamma(3/2 - z/2)}{2\,\Gamma(3/2)} = -\frac{1}{z-3}[1 + (1 - \log 2)(z-3) + O((z-3)^2)],$$

$$L(z) = \frac{\Gamma(3/2 - z/2)}{\Gamma(3/2 + z/2)} \cos\alpha + \sum_{n=2}^{\infty} \frac{\Gamma(n-1)}{\Gamma(n+2)} n^2 \cos(n\alpha) + O(z-3)$$

$$= -\frac{\cos\alpha}{z-3}[1 - (\tfrac{3}{4} - E)(z-3)] + \sum_{n=2}^{\infty} \frac{n}{n^2 - 1} \cos(n\alpha) + O(z-3),$$

where $E = 0.5772\ldots$ is Euler's constant and the final series can be evaluated as

$$\sum_{n=2}^{\infty} \frac{n}{n^2-1} \cos(n\alpha) = \frac{1}{2}\mathrm{Re}\left[\mathrm{e}^{\mathrm{i}\alpha} \sum_{n=1}^{\infty} \frac{\mathrm{e}^{\mathrm{i}n\alpha}}{n} + \mathrm{e}^{-\mathrm{i}\alpha} \sum_{n=3}^{\infty} \frac{\mathrm{e}^{\mathrm{i}n\alpha}}{n} \right]$$

$$= -\cos\alpha \log[2\sin(\alpha/2)] - \tfrac{1}{2} - \tfrac{1}{4}\cos\alpha.$$

Then the residue at $z = 3$ is found to be

$$\mathrm{Res}_{z=3}\left[\frac{\Gamma(z/2)\Gamma(3/2 - z/2)}{2\Gamma(3/2)} L(z) p^{-z} \right] = [\cos\alpha\{\log[\sin(\alpha/2)] + E - \log p\}$$

$$+ \tfrac{1}{2}(1 + \cos\alpha)]p^{-3}. \tag{3.9}$$

(ii) Around $z = 5$ we have the Laurent expansions

$$\frac{\Gamma(z/2)\Gamma(3/2 - z/2)}{2\Gamma(3/2)} = \frac{3/2}{z-5}[1 + (\tfrac{5}{6} - \log 2)(z-5) + O((z-5)^2)],$$

$$L(z) = \frac{\Gamma(3/2 - z/2)}{\Gamma(3/2 + z/2)} \cos\alpha + \frac{\Gamma(5/2 - z/2)}{\Gamma(5/2 + z/2)} \frac{\cos(2\alpha)}{2^{1-z}} + \sum_{n=3}^{\infty} \frac{\Gamma(n-2)}{\Gamma(n+3)} n^4 \cos(n\alpha) + O(z-5)$$

$$= \frac{\cos\alpha}{3(z-5)}[1 - (\tfrac{17}{12} - E)(z-5)] - \frac{4\cos(2\alpha)}{3(z-5)}\left[1 + \left(-\frac{25}{24} + \log 2 + E \right)(z-5) \right]$$

$$+ \sum_{n=3}^{\infty} \frac{n^3}{(n^2-1)(n^2-4)} \cos(n\alpha) + O(z-5),$$

where the final series can be evaluated as

$$\sum_{n=3}^{\infty} \frac{n^3}{(n^2-1)(n^2-4)} \cos(n\alpha)$$

$$= \mathrm{Re}\left[-\tfrac{1}{6}\mathrm{e}^{\mathrm{i}\alpha} \sum_{n=2}^{\infty} \frac{\mathrm{e}^{\mathrm{i}n\alpha}}{n} - \tfrac{1}{6}\mathrm{e}^{-\mathrm{i}\alpha} \sum_{n=4}^{\infty} \frac{\mathrm{e}^{\mathrm{i}n\alpha}}{n} + \tfrac{2}{3}\mathrm{e}^{2\mathrm{i}\alpha} \sum_{n=1}^{\infty} \frac{\mathrm{e}^{\mathrm{i}n\alpha}}{n} + \tfrac{2}{3}\mathrm{e}^{-2\mathrm{i}\alpha} \sum_{n=5}^{\infty} \frac{\mathrm{e}^{\mathrm{i}n\alpha}}{n} \right]$$

$$= \tfrac{1}{3}[\cos\alpha - 4\cos(2\alpha)] \log[2\sin(\alpha/2)] - \tfrac{1}{6} - \tfrac{29}{36}\cos\alpha + \tfrac{1}{18}\cos(2\alpha).$$

Then the residue at $z = 5$ is found to be

$$\operatorname*{Res}_{z=5}\left[\frac{\Gamma(z/2)\Gamma(3/2 - z/2)}{2\Gamma(3/2)} L(z) p^{-z} \right] = [\tfrac{1}{2}[\cos\alpha - 4\cos(2\alpha)]\{\log[\sin(\alpha/2)] + E - \log p\}$$

$$-\tfrac{1}{4} - \tfrac{3}{2}\cos\alpha + (\tfrac{1}{2} - 2\log 2)\cos(2\alpha)]p^{-5}. \quad (3.10)$$

Substitution of (3.9) and (3.10) into (3.8) yields the large-p expansion

$$W(\alpha, p) = p^{-1} - \cos\alpha\{\log[\sin(\alpha/2)] + E - \log p\}p^{-3} - \tfrac{1}{2}(1 + \cos\alpha)p^{-3}$$

$$-\tfrac{1}{2}[\cos\alpha - 4\cos(2\alpha)]\{\log[\sin(\alpha/2)] + E - \log p\}p^{-5}$$

$$+[\tfrac{1}{4} + \tfrac{3}{2}\cos\alpha + (-\tfrac{1}{2} + 2\log 2)\cos(2\alpha)]p^{-5} + O(p^{-7}\log p) \quad (p \to \infty). \quad (3.11)$$

The most interesting feature of (3.11) is the leading term p^{-1} which is absent from the large-p expansion of $W(p)$ as presented in BW (4.9); the latter expansion has a leading term $(-E + 3/2)p^{-3}$. The small-p expansions of $W(\alpha, p)$ and $W(p)$ both have a leading term p^{-1}; see (3.4) and BW (4.22). In both expansions of $W(\alpha, p)$, the pitch dependence is more important than the α-dependence. It has been verified that as $\alpha \downarrow 0$, the large-p expansion (3.11) of $W(\alpha, p)$ becomes the large-p expansion of $W(p)$ from BW (4.9), whereby the limit is taken in conformity with (2.12). A similar check was made for the small-p expansions (3.4) and BW (4.22).

4. The numerical evaluation of $W(\alpha, p)$

The method for numerically evaluating $W(\alpha, p)$ is a straightforward extension of the method described in BW, § 4, for the evaluation of $W(p)$. We write $W(\alpha, p)$ as

$$W(\alpha, p) = \sum_{k=0}^{M-1} A_k(\alpha, p) + W_M(\alpha, p), \quad (4.1)$$

where

$$A_k(\alpha, p) = \frac{1}{2}\int_0^{\pi} \sin^2 t[\{p^2(t + k\pi + \alpha/2)^2 + \sin^2 t\}^{-3/2}$$

$$+\{p^2(t + k\pi - \alpha/2)^2 + \sin^2 t\}^{-3/2}]\,\mathrm{d}t \quad (4.2)$$

and

$$W_M(\alpha, p) = \frac{1}{2}\int_{M\pi}^{\infty} \sin^2 t[\{p^2(t+\alpha/2)^2 + \sin^2 t\}^{-3/2} + \{p^2(t-\alpha/2)^2 + \sin^2 t\}^{-3/2}]\,\mathrm{d}t. \quad (4.3)$$

Here, M is an integer such that $(M\pi - \alpha/2)p > 1$. The integrals $A_k(\alpha, p)$ are calculated by adaptive quadrature, while $W_M(\alpha, p)$ is evaluated by an analytic approximation.

p	$W(p)$	$W(\pi/2,p)$	$W(2\pi/3,p)$	$W(\pi,p)$
0.01	0.957022×10^{2}	0.996535×10^{2}	0.994508×10^{2}	0.993069×10^{2}
0.05	0.173173×10^{2}	0.196546×10^{2}	0.194523×10^{2}	0.193086×10^{2}
0.1	0.801822×10^{1}	0.965819×10^{1}	0.945703×10^{1}	0.931407×10^{1}
0.2	0.370710×10^{1}	0.467226×10^{1}	0.447767×10^{1}	0.433908×10^{1}
0.3	0.239240×10^{1}	0.302815×10^{1}	0.284996×10^{1}	0.272379×10^{1}
0.4	0.174543×10^{1}	0.222381×10^{1}	0.206975×10^{1}	0.196213×10^{1}
0.5	0.134138×10^{1}	0.175584×10^{1}	0.162671×10^{1}	0.153777×10^{1}
0.6	0.105695×10^{1}	0.145425×10^{1}	0.134689×10^{1}	0.127372×10^{1}
0.7	0.844909	0.124544×10^{1}	0.115576×10^{1}	0.109502×10^{1}
0.8	0.682350	0.109273×10^{1}	0.101707×10^{1}	0.965957
0.9	0.555822	0.976115	0.911533	0.867901
1.0	0.456367	0.883919	0.828167	0.790427
2.0	0.928365×10^{-1}	0.468166	0.448986	0.435385
3.0	0.308916×10^{-1}	0.321010	0.311638	0.304712
4.0	0.136084×10^{-1}	0.244085	0.238716	0.234623
5.0	0.711198×10^{-2}	0.196740	0.193348	0.190702
6.0	0.416244×10^{-2}	0.164690	0.162397	0.160576
7.0	0.263927×10^{-2}	0.141572	0.139943	0.138630
8.0	0.177602×10^{-2}	0.124120	0.122917	0.121935
9.0	0.125119×10^{-2}	0.110482	0.109567	0.108812
10.0	0.914128×10^{-3}	0.995357×10^{-1}	0.988208×10^{-1}	0.982267×10^{-1}

TABLE 1. Numerical evaluation of $W(p)$ and $W(\alpha,p)$ for $\alpha=\pi/2$, $2\pi/3$, π, and the values of p indicated. The results for $W(p)$ were taken from BW, table 1.

The quadrature is based on repeated bisection of the interval of integration $[0,\pi]$ using the Gauss–Kronrod rule as described in BW. To obtain an approximation for $W_M(\alpha,p)$, the integrand in (4.3) is expanded in powers of p^{-1} and the power series is integrated term by term. Only the first two terms are retained and these terms are further evaluated through repeated integration by parts. As a result we find

$$W_M(\alpha,p)=\tfrac{1}{2}(B_0^+ + B_0^-)p^{-3}-\tfrac{3}{4}(B_1^+ + B_1^-)p^{-5}+\Delta, \tag{4.4}$$

where Δ is the error, and

$$B_0^{\pm}=\tfrac{1}{4}(M\pi\pm\alpha/2)^{-2}-\tfrac{3}{8}(M\pi\pm\alpha/2)^{-4}+\tfrac{15}{8}(M\pi\pm\alpha/2)^{-6}, \tag{4.5}$$

$$B_1^{\pm}=\tfrac{3}{32}(M\pi\pm\alpha/2)^{-4}-\tfrac{75}{128}(M\pi\pm\alpha/2)^{-6}. \tag{4.6}$$

The results (4.4), (4.5) and (4.6) correspond to BW (4.35), (4.38) and (4.40), respectively. From the error analysis in BW, §4, which gives an upper bound for Δ, it follows that an accuracy of six significant digits can be achieved by selecting M as the smallest integer such that $M\pi-\alpha/2\geqslant 10$ and $(M\pi-\alpha/2)p\geqslant 10$.

For the same values of p as in table 1 of BW, the present table 1 gives $W(p)$ and $W(\alpha,p)$ for $\alpha=\pi/2$, $2\pi/3$ and π. Table 2 contains the numerical results based on the asymptotic expansions (3.4) and (3.11), where in (3.4) we employ the additional results from (3.5) and (3.6). A comparison between tables 1 and 2 shows that the small-p expansion (3.4) reproduces six correct significant digits when $p\leqslant 0.1$. For increasing p and increasing α the accuracy of the small-p expansion decreases. For example, at $p=0.4$, five correct significant digits are reproduced when $\alpha=\pi/2$, whereas the expansion is accurate to 1.2% when $\alpha=2\pi/3$, and to 2.5% when $\alpha=\pi$. Similarly, the large-p expansion (3.11) is accurate to within 1% for $p\gtrsim 3$. The values of α considered

p	$W(\pi/2, p)$	$W(2\pi/3, p)$	$W(\pi, p)$
0.01	0.996535×10^2	0.994508×10^2	0.993069×10^2
0.05	0.196546×10^2	0.194523×10^2	0.193086×10^2
0.1	0.965819×10^1	0.945703×10^1	0.931407×10^1
0.2	0.467226×10^1	0.447747×10^1	0.433866×10^1
0.3	0.302817×10^1	0.285146×10^1	0.272669×10^1
0.4	0.222387×10^1	0.209508×10^1	0.201209×10^1
0.5	0.175463×10^1	0.174266×10^1	0.176851×10^1
0.6	0.144401×10^1	0.169099×10^1	0.196752×10^1
0.7	0.120222×10^1	0.197464×10^1	0.277188×10^1
0.8	0.962095	0.272237×10^1	0.451371×10^1
0.9			
1.0			
2.0	0.446522	0.429129	0.465086
3.0	0.319340	0.309927	0.307161
4.0	0.243823	0.238426	0.235028
5.0	0.196679	0.193276	0.190800
6.0	0.164672	0.162375	0.160607
7.0	0.141566	0.139935	0.138642
8.0	0.124117	0.122913	0.121940
9.0	0.110481	0.109565	0.108814
10.0	0.995351×10^{-1}	0.988200×10^{-1}	0.982279×10^{-1}

TABLE 2. Asymptotic expansions for $W(\alpha, p)$ with $\alpha = \pi/2$, $2\pi/3$ and π. The results for pitch values up to and including 0.8 are based on the small-p expansion (3.4); the remaining entries are based on the large-p expansion (3.11).

are sufficient to calculate the vortex velocity for the cases of $N = 1, 2, 3$, and 4 vortices, as explained in § 5.2. These values of N cover the majority of applications.

5. Application of the analysis

At a sufficiently large distance behind propellers, wind turbines and hovering, ascending or descending rotors – in the so-called 'far wake' – the vorticity is concentrated in N helical tip vortices each of strength Γ, where N is the number of blades. In addition, there are N hub vortices of the same strength lying along the axis of rotation. This arrangement of vorticity, with constant pitch, p, and radius R, is the simplest possible and allows the application of the analysis developed in the previous sections. (Of course, the cores of the vortices must continue to grow, but we will defer discussion of this issue.) The circulation Γ in the Biot–Savart expression (2.7) is taken as positive when power is added to the flow, and negative for wind turbines. The vortex radius R, introduced in § 2, is now also the radius of the far wake. Note that the vortex pitch p, defined in (2.2), is dimensionless. In terms of R_T, the blade radius, one has $R < R_T$ for rotors and propellers, but $R > R_T$ for wind turbines.

5.1. *Preliminaries: average velocity and importance of small pitch in the far wake*

To apply the present analysis, we need a further result for $\bar{U}$, the average velocity within the far wake in the direction of the rotor's axis of rotation. This result is

$$\frac{\bar{U}}{\Omega R_T} = \frac{N\Gamma/(\Omega R_T^2)}{2\pi p R/R_T} \tag{5.1}$$

for hovering rotors. In (5.1), $\bar{U}$ and Γ are normalized by Ω, the angular velocity of the rotor, and R_T. These are the usual quantities used for normalization of the results of hovering rotor experiments. For wind turbines and propellers

$$\frac{\bar{U}}{U_0} = 1 + \frac{N\Gamma/(U_0 R_T)}{2\pi p R/R_T}. \tag{5.2}$$

In (5.2), $\bar{U}$ is normalized by U_0, the wind speed or forward speed of the propeller, and lengths are normalized by R_T. The scaling used in (5.2) is the conventional one for wind turbines and propellers. Because it differs from that used for rotors, we have decided to include the appropriate normalizations for Γ and other quantities in the expressions, such as (5.1) and (5.2), rather than to introduce new symbols for differently scaled quantities.

The result (5.1) can be derived in a number of ways. It is a direct consequence of Hardin's solution (1982, formula (8)) which is discussed in Appendix A. Note that the term S_1 in Hardin's solution does not contribute to the average velocity. The result (5.1) can also be obtained by the following simple argument. Consider a rectangular contour with sides $2\pi pR$ placed along and parallel to the axis of rotation, and radial extent r. When $r > R$, and the contour encloses N tip vortices without intersecting them, the area integral of the vorticity within the contour is $N\Gamma$, and the contributions to the circulation around the rectangle from the two radial legs cancel. Thus the circulation is $2\pi pR\bar{U}$, where $\bar{U}$ is, for the moment, the velocity along the axis. Equating the vorticity integral and the circulation gives (5.1) and the extension to (5.2), by including the wind speed or forward speed of the propeller, is straightforward. When $r < R$, there is no circulation around the contour, showing that $\bar{U}$ is independent of radius in the far wake. Thus a far wake containing helical tip vortices and straight hub vortices is consistent with the one-dimensional analysis that leads, for example, to the Betz limit on the power output of wind turbines. It will be shown in § 5.3 that considerations of the tip vortex pitch and velocity lead to an expression for the bound vorticity of each blade, when the turbine is operating at the Betz limit.

Most wake vortices have small pitch. For wind turbines, we assume for the present that the axial velocity of a tip vortex in the far wake, U, is given by $U = (U_0 + \bar{U})/2$, and the circumferential velocity is $\lambda R U_0/R_T$, where λ is the tip speed ratio, that is, the circumferential velocity of the blade tip divided by the wind speed. If the tip vortex is force-free, then

$$p = \frac{1 + \bar{U}/U_0}{2\lambda R/R_T}. \tag{5.3}$$

Now the one-dimensional analysis that leads to the Betz limit is reasonably accurate near the point of maximum power production (see e.g. Spera 1994), and $\bar{U}/U_0 \approx 1/3$ and $R/R_T \approx 2$ at this point. Thus we obtain

$$p \approx \frac{1}{3\lambda}. \tag{5.4}$$

For most two- and three-bladed turbines, maximum power production occurs when λ is in the range of 7–10. Taking the lower value gives $p \approx 0.05$.

There are much more experimental data available for hovering rotors, so that estimates of magnitude are not needed. For example, the experiment of Leishman, Baker & Coyne (1996) with a one-bladed rotor gave $p = 0.053$ – see their table 2, where pR/R_T and R/R_T appear as k_2 and A, respectively.

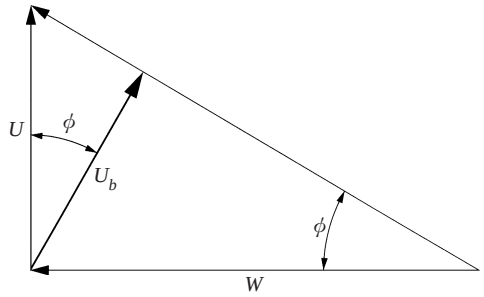

FIGURE 1. The geometric relationship of the velocities in (5.5) and (5.6). Note that $\phi = \arctan p$.

5.2. *The velocity of propagation of N vortices in the far wake*

Consider again the arrangement of N identical helical vortices, spaced $2\pi/N$ radians apart. The binormal velocity U_b induced at any of the helices is given by the sum of the self-induced component, as determined by BW, and the contributions of the remaining $N-1$ vortices, found in § 2. However, as suggested by the appearance of the axial velocity of the tip vortex in (5.3), it is not the binormal velocity that is most useful in practice; rather it is the axial and circumferential velocities, U and W, respectively. We now determine U_b, U and W. If the far wake is force-free, then U is *not* the axial component of U_b, for the reason given by Saffman (1992, § 11.2) in his analysis of a helix of large pitch. Any difference between the velocity of a material point on the vortex and the self-induced velocity must lie in the direction of the helix. Furthermore, U and W are related kinematically to σ, the rate of rotation of the helix. Thus

$$U = pR\sigma = (p^2+1)^{1/2}U_b \tag{5.5}$$

and

$$W = R\sigma. \tag{5.6}$$

The relationship of U_b to U and W is illustrated in figure 1. We now determine U_b, beginning with BW (3.5) for the self-induced contribution in the form of C_{MS}; here, the subscript denotes that the result stems from applying the Moore–Saffman procedure, as described in Ricca (1994, § 3) using the same notation. By adding the contributions of the remaining $N-1$ vortices, we find

$$U_b = \frac{\Gamma}{4\pi R}\left[\sum_{j=1}^{N-1} I_b\left(\frac{2\pi j}{N}, p\right) + \frac{C_{MS}}{p^2+1} + \frac{1}{p^2+1}\log\frac{1}{\varepsilon}\right],$$

where I_b is given by (2.8). Here, we also included the contribution from the curvature singularity, which in the Moore–Saffman procedure is provided by the osculating circular vortex whose radius is the radius of curvature of the helix. The curvature term involving $\varepsilon = a/[(p^2+1)R]$, where a is the vortex core radius, stems from Ricca (1994, formula (3.14)). The term involving summation represents the effects of the extra $N-1$ vortices. This term will be zero in the case of a single helix ($N = 1$). Substitution of (2.9) and BW (3.5) gives

$$U_b = \frac{\Gamma}{4\pi R}\left[(p^2+1)^{1/2}\left\{W(p) + \sum_{j=1}^{N-1} W\left(\frac{2\pi j}{N}, p\right)\right\} - \frac{2Np}{(p^2+1)^{1/2}}\right.$$
$$\left. + \frac{1}{p^2+1}\{-\tfrac{1}{4} + \log 2 + 2p^2 - \tfrac{1}{2}\log(p^2+1)\} + \frac{1}{p^2+1}\log\frac{1}{\varepsilon}\right], \tag{5.7}$$

where $W(p)$ and $W(\alpha, p)$ are given by (2.1) and (2.10). The osculating vortex must satisfy $\varepsilon \ll 1$, and is assumed to have uniform vorticity, but it appears that the details of the vortex structure only have a small effect on its binormal velocity. This is demonstrated by BW who establish the small difference between C_{MS} and C_H where the latter is determined from Hardin's (1982) analysis for a line vortex. Furthermore, the vortex structure cannot influence the contributions from the remaining $N-1$ vortices, provided $\varepsilon \ll 1$, and presumably, $a/p \ll 1$.

Using the results of table 1 in (5.7) allows U_b to be evaluated for a wide range of pitch values. Next, U and W are simply determined by means of (5.5) and (5.6). At sufficiently small pitch, U_b can also be found from its small-p expansion

$$U_b = \frac{\Gamma}{4\pi R}\left[Np^{-1}(p^2+1)^{1/2} - \frac{\log(N/p)}{p^2+1} + \frac{3}{4} - \frac{2Np}{(p^2+1)^{1/2}} + \left(\frac{3}{8}\frac{\zeta(3)}{N^2} - \frac{5}{4}\right)p^2 + O(p^4)\right] \quad (p \downarrow 0) \quad (5.8)$$

where the curvature term has been deleted. The expansion (5.8) is obtained by inserting into (5.7) the small-p expansions of $W(\alpha, p)$ and $W(p)$ from (3.4) and BW (4.22), followed by the use of (3.7) to simplify the sum of Clausen functions Cl_3. Likewise, the large-p expansion of U_b can be found from (5.7) by inserting the large-p expansions of $W(\alpha, p)$ and $W(p)$ from (3.11) and BW (4.9).

5.3. *Comparison with experiments*

By setting $W(\alpha, p) \approx p^{-1}$ and $W(p) \approx p^{-1}$, which are the leading terms in the small-p expansions (3.4) and BW (4.22), we have, to leading order, for small p,

$$\frac{U}{\Omega R_T} = \frac{N\Gamma/(\Omega R_T^2)}{4\pi pR/R_T} = \frac{\bar{U}}{2\Omega R_T} \quad (5.9)$$

by (5.1) for hovering rotors, and

$$\frac{U}{U_0} = 1 + \frac{N\Gamma/(U_0 R_T)}{4\pi pR/R_T} = \frac{1+\bar{U}/U_0}{2} \quad (5.10)$$

by (5.2) for wind turbines and propellers.

Note that (5.10) was used as a preliminary in obtaining the estimate (5.3). Thus, we find that the usual assumption that the axial velocity of the vortex is the average of the velocities within and outside the wake, is only an approximation and can only be justified at sufficiently small pitch.

We now compare (5.7) with the available experimental data, beginning with the single, hovering rotor data of Leishman *et al.* (1996), mentioned earlier. For $N = 1$ we have

$$U = \frac{\Gamma}{4\pi R(p^2+1)^{1/2}}\left[C_{MS} + \log\frac{1}{\varepsilon}\right]. \quad (5.11)$$

Now we assume that the angular velocity of the vortex (σ in (5.5), (5.6)) is also the angular velocity of the rotor, Ω, so that $pR = U/\Omega$ from (5.5). To eliminate Γ from (5.11) we use (5.1) with $N = 1$, for the average velocity in the far wake. By combining these results we find

$$\frac{2\Omega R}{\bar{U}} = \frac{1}{(p^2+1)^{1/2}}\left[C_{MS} + \log\frac{1}{\varepsilon}\right]. \quad (5.12)$$

From Leishman *et al.* (1996, figure 7), the velocity in the wake is reasonably uniform

with radius, and $\bar{U}/U_0 \simeq 0.073$ when $x/R_T = 0.399$, where x is the streamwise coordinate originating at the blades, the furthest downstream position measured. However, the relation between the wake radius and the vortex age in Leishman *et al.* (1996, formula (2)), indicates that the wake has not contracted fully by this position. From this relation and employing conservation of mass, we may estimate $\bar{U}/(\Omega R_T) \approx 0.0786$. From Leishman *et al.* (1996, figure 14) we judge that $\varepsilon \approx 0.0161$ in (5.12). Furthermore, $R/R_T = 0.78$ from Leishman *et al.* (1996, table 2) which fixes the left-hand side of (5.12). Using the small-p expansion of C_{MS} from BW (4.23), the expression (5.12) can be written as a nonlinear equation in p. As demonstrated in BW, table 1, the small-p expansion is accurate to six digits up to $p \sim 0.05$. Solving the equation by use of a standard root-finding algorithm gives $pR/R_T = 0.0436$, compared to the measured value of 0.041 recorded as k_2 in Leishman *et al.* (1996, table 2). In order to make pR/R_T equal to the measured k_2, the value of ε would have to be increased to 0.045, which is unrealistically large. If we ignore the curvature term and take into account only the p^{-1}-term in the expansion of C_{MS}, then the estimate for pR/R_T changes to $pR/R_T = \bar{U}/(2\Omega R_T) = 0.0393$, which is 10% smaller than the higher-order estimate. This is due partly to a partial cancellation of the curvature term by the higher-order pitch terms. Thus the approximations embodied in (5.9) and (5.10) appear to be reasonably accurate at typical values of pitch for hovering rotors and wind turbines. Substitution into (5.1) of $\bar{U}$ estimated as described above and of the measured value $pR/R_T = 0.041$ provides an estimate for the circulation Γ. This gives $\Gamma/(\Omega R_T^2) = 0.020$ which compares to values around 0.012 determined from the circulation around the tip vortices; see Leishman *et al.* (1996, figure 13) and Bhagwat & Leishman (2000*a*, figure 14). Interestingly, the estimate is closer to the measured bound circulation of the blade; see e.g. Bhagwat & Leishman (2000*a*, figure 8). Unfortunately, there are no far-wake data for wind turbines with which to compare the present analysis.

Propellers tend to involve pitch values larger than those in the far wakes of hovering rotors and wind turbines. Favier & Maresca (1984) and Favier, Ettaouil & Maresca (1989) present tip vortex and other measurements in the wake of a four-bladed propeller for a wide range of operating conditions. For a blade mean pitch angle of 32.5° and advance ratio $J = \pi/\lambda = 0.89$, Favier & Maresca (1984, figure 14) gives $pR/R_T = 0.337$, or $p = 0.383$ by use of Favier & Maresca (1984, formula (1)) for the wake contraction which gives $R/R_T = 0.879$. The value of p is too large for the small-p expansion to be accurate. The sum in (5.7) was evaluated numerically for $p = 0.383$ and the curvature term ignored, leading to

$$\frac{U}{U_0} = 1 + 0.5862\frac{\Gamma}{U_0 R} = \frac{p\lambda R}{R_T} = 1.19, \tag{5.13}$$

using (5.3), (5.5) and (5.10). Here, U_0 is the forward speed of the propeller (17.2 m s^{-1}). This gives $\Gamma/(\Omega R_T^2) = 0.080$. The circulation was not measured in these experiments, but Favier *et al.* (1989, figure 11*a*) shows the computationally predicted bound circulation for this operating condition. The maximum value of $\Gamma/(\Omega R_T^2)$ is 0.045, which compares to the estimate of 0.050 in Favier & Maresca (1984, figure 25) for the same operating conditions.

From the comparison with the measurements behind a hovering rotor and a propeller, it appears that the present analysis overestimates the circulation of the tip vortex. There are at least two possible reasons for this. First, the curvature term would act to reduce the estimated Γ for the propeller, for which the core radius was not measured. To reduce $\Gamma/(\Omega R_T^2)$ from 0.080 to 0.050, however, would require $\varepsilon \approx 0.009$

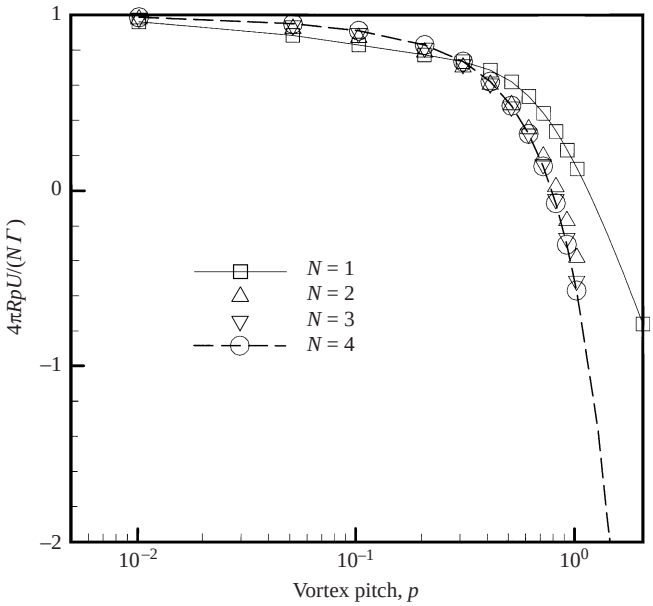

FIGURE 2. The axial velocity of N vortices as a function of their pitch. For visual aid, the solid and dashed lines join the results for $N = 1$ and $N = 4$, respectively.

in (5.7), which would appear to be unrealistically small. Secondly, and more likely, the assumed wake structure is too simplistic, in that some vorticity in the actual wake lies outside the tip and hub vortices. The significant radial variation in the axial velocity profiles in Favier & Maresca (1984, figure 17) suggests strongly that this is the case.

We now discuss the effect of N on the vortex velocity and investigate the range of p over which the approximation leading to (5.9) and (5.10) may be made. The axial velocity U calculated from (5.5) and (5.7) without the curvature term, by use of the results in table 1, is shown in figure 2. The ratio $4\pi RpU/(N\Gamma)$ is plotted as a function of the vortex pitch p, for $N = 1$, 2, 3 and 4. This ratio is unity if the expression between the square brackets in (5.7) is equal to N/p. Using (5.8) for U_b at small pitch gives the following small-p expansion:

$$\frac{4\pi RpU}{N\Gamma} = 1 - \frac{p}{N}\frac{\log(N/p)}{(p^2+1)^{1/2}} + \frac{3}{4}\frac{p}{N} - p^2 + \frac{1}{N}\left(\frac{3}{8}\frac{\zeta(3)}{N^2} - \frac{7}{8}\right)p^3 + O(p^5) \quad (p \downarrow 0). \tag{5.14}$$

For example, at $p = 0.05$, the ratio increases from 0.88 for $N = 1$ to 0.95 for $N = 4$. Generally, the accuracy of (5.9) and (5.10) increases with increasing N, but by far the largest change occurs between $N = 1$ and $N = 2$. Including the effects of curvature means that U will be slightly less than indicated by the right-hand side of (5.9) where Γ is positive, but greater than (5.10) for wind turbines. The relatively small effect of the vortex core radius on the induced velocity means that the effects of its growth, which must continue in the far wake while the vortex radius and pitch remain constant, will always be of higher order. In practical terms, the far wake must exist over a sufficiently large distance for its effects on the blades to be representable by a wake of infinite extent. It may well be that the far wake eventually succumbs to an

instability much like the long-wavelength Crow instability of aircraft trailing vortices, as suggested by the calculations of Gupta & Loewy (1974) and Bhagwat & Leishman (2000*b*).

There does not appear to be any necessary connection between σ and Ω (the angular velocities of the vortex and the rotor, respectively), even though their equality is assumed in all experimental studies, and has been assumed in the analysis above. That some caution is needed in making that assumption, is indicated by U changing sign in figure 2 at around $p = 1$ for all values of N. In other words, helices of small pitch rotate in the opposite direction to those at larger pitch. It is likely that there is a range of p for which the approximation $\sigma = \Omega$ is valid and this range is a subset of that for which $U \sim p^{-1}$. Experimentally, data sampling is usually triggered by a blade passing an arbitrary point, allowing the three-dimensional structure to be obtained from ensemble averages of the stationary measurements. The product of Ω and the time after triggering is assumed to be the azimuthal 'location' of the measurement relative to the position of the blade at triggering. Any consistent difference between σ and Ω would prevent the details of the tip vortices from appearing in the ensemble averages, except in the unlikely event that σ were an integer multiple of Ω.

Assuming that $\sigma = \Omega$, and that U is sufficiently well represented by the leading p^{-1}-term of its small-p expansion, the present analysis can be used in another way to estimate Γ for wind turbines. By combining (5.2) and (5.3), it follows that

$$\frac{\bar{U}}{U_0} = \sqrt{1 + \frac{N\lambda\Gamma/(U_0 R_T)}{\pi}}. \tag{5.15}$$

To optimize power output, for example, we set $\bar{U}/U_0 = 1/3$ and obtain

$$\frac{\Gamma_m}{U_0 R_T} = -\frac{8\pi}{9N\lambda_m}, \tag{5.16}$$

where the subscript m indicates values for maximum performance. In other words, having chosen N and λ_m, the expression (5.16) determines the circulation required for optimum performance. The result (5.16) can also be derived from an entirely different basis by balancing the axial momentum in the air flowing over the blades against the lift generated on an 'ideal rotor'. As shown in Spera (1994, equation (5–44)), the result is equivalent to (5.16). This provides further evidence of the consistency between the analysis of multiple helical vortices and the behaviour of simple wakes.

5.4. *The accuracy of wake modeling*

Even in sophisticated computer models of wind turbines, propellers, and rotors, the vorticity in the far wake is often represented by straight vortex segments. For example, Xu & Sankar (2000) describe a computational study of wind turbines in which a 'Navier–Stokes' solution in the vicinity of the blades is combined with an 'inviscid zone' including the far wake where the vorticity is represented by freely convecting straight segments. Similar segments were used in the study of the stability of helical vortex wakes by Bhagwat & Leishman (2000*b*). The straight-segment approximation is computationally attractive, but has often been criticised on the grounds that the curvature singularity is not automatically captured. This has led to the formulation of more complex alternatives, such as the 'basic curved vortex segment' of Bliss, Teske & Quackenbush (1987). Its accuracy was assessed largely by comparison with the velocity field of vortex rings: the translation of vortex rings is due almost entirely to the curvature term. However, the present study suggests that the curvature term is

rarely dominant for single and multiple helical vortices, so the comparison may well be inappropriate.

The results of table 1 were used to assess the accuracy of the straight-segment approximation over a wide range of pitch, Wood & Li (2001). A simple correction was developed for the effects of vortex curvature on the self-induced velocity. The error in the approximation at small pitch was caused mainly by the segments that end or begin in line with the point at which the velocity is to be determined. These segments do not contribute to U_b. As a consequence, the straight-segment approximation is only first-order accurate at small numbers of, say, segments per revolution of the helix, improving to third order at much higher numbers. Neither of these results is obtainable by comparison to the velocity field of a vortex ring, for which the straight-segment approximation is second-order accurate, e.g. Bhagwat & Leishman (2001*b*).

6. Conclusions

In this paper we have extended the determination of the velocity of a single, constant-diameter helical vortex to include the effects of $N-1$ additional helical vortices, spaced $2\pi/N$ radians apart, where $N \geqslant 2$. This arrangement approximates the tip vortices in the far wake of wind turbines, propellers, and ascending, descending, or hovering rotors, where N is the number of blades.

The contributions from the additional vortices are determined from a straightforward application of the Biot–Savart law, resulting in an infinite integral – for $W(\alpha, p)$ in (2.10) – that, apparently, cannot be evaluated in closed equation Based on a Mellin–Barnes integral representation of $W(\alpha, p)$, the asymptotic expansions are determined for small and for large pitch, p. At large pitch, the Kelvin limit, the additional vortices make a significant change to the induced velocity in that the leading term in $W(\alpha, p)$ at large pitch is p^{-1} from (3.11), whereas the leading term in $W(p)$ is proportional to p^{-3} from BW (4.9). At small pitch, the leading p^{-1}-term found for a single vortex carries over to a term N/p for multiple vortices. The spacing does not have a significant effect, partly because of the symmetry constraint of (2.11) which means, for example, that the second and fourth vortices induce the same velocity on the first when $N = 4$.

It is demonstrated that the small-p limit is of practical significance for wind turbine and hovering rotor applications. Much more experimental information is available for the latter case and it is shown that the present analysis predicts the vortex pitch and circulation with reasonable accuracy. It is also shown that a wake consisting only of helical tip vortices and hub vortices lying along the axis of rotation is consistent with the one-dimensional wake analysis used to determine propeller thrust and wind turbine power output. If the pitch is small enough for the term N/p to dominate the vortex velocity, then that velocity is the average of the mean velocity inside and the velocity outside the wake. For a wind turbine, this leads to the simple expression (5.16) for the bound circulation when the power output is maximized. The result (5.16) can also be derived from a completely different basis: simple blade-element theory combined with one-dimensional wake analysis. This coincidence provides further evidence of the consistency of the present analysis with the standard methods of evaluating turbine performance.

The comparison of the present analysis to the available experimental data concentrated on the case of small values of the pitch. There were, however, three areas where larger values of p are important. The first was in the propeller experiment considered in § 5.3; most propeller applications involve values of p for which the

small-p approximation for the vortex velocity is not sufficiently accurate. Secondly, figure 2 shows that the vortex velocity changes sign with increasing pitch for all values of N ($\leqslant 4$) that were considered. Since the sign of U is equal to the sign of σ on account of (5.5), the direction of rotation of the vortices must also change. Therefore the commonly assumed equality between the angular velocities of the blades and of the helical vortices they produce, is not universally valid. Thirdly, it was pointed out in § 5.4 that the results in table 1 can be used to assess the accuracy of various discretization schemes employed to model trailing helical vortices in free-wake computer models of wind turbines, propellers and rotors.

D. H. W.'s contribution was supported by the Australian Research Council. We thank Professor J. G. Leishman and Dr Christian Maresca for their comments on the applications of the analysis.

Appendix A. The induced velocity from Hardin's (1982) solution

It is shown here that Hardin's (1982) solution for the interior flow (radius $r < 1$) of a helical line vortex is reducible to (2.9). Take $r = 1 - \varepsilon$ where ε is the positive radial distance from the point at which the velocity is required, to the helix. This definition of ε is not to be confused with that used in § 5. The current definition is the only one used in this Appendix, and is not used elsewhere. Hardin's solution (1982, formula (8)) involves the Kapteyn series

$$S_1(R(1-\varepsilon),\alpha) = \sum_{m=1}^{\infty} mK'_m(m/p)I_m((1-\varepsilon)m/p)\cos(m\alpha), \tag{A 1}$$

where $I_m(\cdot)$ and $K_m(\cdot)$ are modified Bessel functions of order m and the prime denotes differentiation with respect to the argument. Introduce the notation

$$S(a,b,\alpha) = \sum_{m=1}^{\infty} K_m(ma)I_m(mb)\cos(m\alpha), \quad a > b \geqslant 0. \tag{A 2}$$

Then $S_1(R(1-\varepsilon),\alpha)$ is equal to $\partial S(a,b,\alpha)/\partial a$ with $a = 1/p$, $b = (1-\varepsilon)/p$. By an analysis similar to that of Boersma & Yakubovich (1998) we deduce

$$S(a,b,\alpha) = \frac{1}{4}\sum_{\pm}\int_0^{\infty}[t^2+a^2+b^2-2ab\cos(t\pm\alpha)]^{-1/2}\,\mathrm{d}t - \frac{1}{2\pi}\int_0^{\infty}\mathrm{d}t\int_0^{\pi}(t^2+a^2+b^2-2ab\cos s)^{-1/2}\,\mathrm{d}s. \tag{A 3}$$

Differentiation with respect to a yields

$$\frac{\partial S(a,b,\alpha)}{\partial a} = -\frac{1}{4}\sum_{\pm}\int_0^{\infty}\frac{a-b\cos(t\pm\alpha)}{[t^2+a^2+b^2-2ab\cos(t\pm\alpha)]^{3/2}}\,\mathrm{d}t + \frac{1}{2\pi}\int_0^{\infty}\mathrm{d}t\int_0^{\pi}\frac{a-b\cos s}{(t^2+a^2+b^2-2ab\cos s)^{3/2}}\,\mathrm{d}s. \tag{A 4}$$

The second (double) integral has the value $1/2a$ according to Boersma & Yakubovich (1998), while the first term can be rewritten to give

$$\frac{\partial S(a,b,\alpha)}{\partial a} = \frac{1}{2a} - \frac{1}{4}\int_{-\infty}^{\infty}\frac{a-b\cos(t+\alpha)}{[t^2+a^2+b^2-2ab\cos(t+\alpha)]^{3/2}}\,\mathrm{d}t. \tag{A 5}$$

Substitute $a = 1/p$, $b = (1-\varepsilon)/p$, or rather $b = 1/p$, since $\varepsilon \downarrow 0$. Then we obtain

$$\lim_{\varepsilon\downarrow 0} S_1(R(1-\varepsilon),\alpha) = \frac{p}{2} - \frac{1}{4}\int_{-\infty}^{\infty} \frac{(2/p)\sin^2((t+\alpha)/2)}{[t^2+(4/p^2)\sin^2((t+\alpha)/2)]^{3/2}}\,\mathrm{d}t$$

$$= \frac{p}{2} - \frac{p^2}{8}\int_{-\infty}^{\infty} \frac{\sin^2(t+\alpha/2)}{[\,p^2t^2+\sin^2(t+\alpha/2)]^{3/2}}\,\mathrm{d}t$$

$$= \frac{p}{2} - \frac{p^2}{4}W(\alpha,p), \tag{A 6}$$

on account of (2.10). Hardin's solution (1982, equation (8)) comprises expressions for the velocity components u_ϕ, w, in cylindrical coordinates in terms of S_1. By changing to our notation it is found that $I_b(\alpha,p)$ in (2.7) is given by

$$I_b(\alpha,p) = \frac{w-pu_\phi}{(p^2+1)^{1/2}}\bigg/\frac{\Gamma}{4\pi R} = \frac{2}{(p^2+1)^{1/2}}\left[\frac{1}{p} - \frac{2(p^2+1)}{p^2}S_1\right]. \tag{A 7}$$

Finally, by inserting the value of S_1 from (A 6) we recover (2.9).

Appendix B. A Mellin–Barnes integral representation of $W(\alpha,p)$

By use of

$$\frac{\sin^2(t+\alpha/2) - t\sin(t+\alpha/2)\cos(t+\alpha/2)}{[\,p^2t^2+\sin^2(t+\alpha/2)]^{3/2}} = \frac{\mathrm{d}}{\mathrm{d}t}\left[\frac{t}{[\,p^2t^2+\sin^2(t+\alpha/2)]^{1/2}}\right]$$

in the integrand of (2.10), we express the integral $W(\alpha,p)$ as

$$W(\alpha,p) = \frac{1}{p} + \frac{1}{2}\int_{-\infty}^{\infty} \frac{t\sin(t+\alpha/2)\cos(t+\alpha/2)}{[\,p^2t^2+\sin^2(t+\alpha/2)]^{3/2}}\,\mathrm{d}t$$

$$= \frac{1}{p} + W_1(p) + W_2(p), \tag{B 1}$$

where

$$W_1(p) = \frac{1}{2}\int_0^{\pi}\left\{\frac{t\sin(t+\alpha/2)\cos(t+\alpha/2)}{[\,p^2t^2+\sin^2(t+\alpha/2)]^{3/2}} + \frac{t\sin(t-\alpha/2)\cos(t-\alpha/2)}{[\,p^2t^2+\sin^2(t-\alpha/2)]^{3/2}}\right\}\mathrm{d}t \tag{B 2}$$

and $W_2(p)$ is the integral over $[\pi,\infty)$ with the same integrand. Proceeding as in BW, §4, we determine the Mellin transforms of $W_1(p)$ and $W_2(p)$, defined by

$$\mathscr{M}\{W_{1,2}(p)\} = \int_0^{\infty} W_{1,2}(p)p^{z-1}\,\mathrm{d}p \tag{B 3}$$

for complex z. As a preliminary we establish the auxiliary result

$$\mathscr{M}\{(p^2+a^2)^{-v}\} = a^{z-2v}\frac{\Gamma(z/2)\Gamma(v-z/2)}{2\Gamma(v)}, \tag{B 4}$$

valid for $0 < \mathrm{Re}(z) < 2v$. Here, $\Gamma(\cdot)$ denotes the gamma function. By use of (B 4) with $v = 3/2$ we find

$$\mathscr{M}\{W_{1,2}(p)\} = \frac{\Gamma(z/2)\Gamma(3/2-z/2)}{2\Gamma(3/2)}L_{1,2}(z), \tag{B 5}$$

where

$$L_1(z) = \frac{1}{2}\int_0^{\pi} \big\{\sin(t+\alpha/2)\cos(t+\alpha/2)|\sin(t+\alpha/2)|^{z-3} + \sin(t-\alpha/2)\cos(t-\alpha/2)|\sin(t-\alpha/2)|^{z-3}\big\}\frac{\mathrm{d}t}{t^{z-1}} \quad (B\,6)$$

and $L_2(z)$ is the integral over $[\pi,\infty)$ with the same integrand. The integrals for $L_1(z)$ and $L_2(z)$ are convergent for $1 < \mathrm{Re}(z) < 3$ and $\mathrm{Re}(z) > 2$, respectively. Accordingly, $L_1(z)$ is analytic for $1 < \mathrm{Re}(z) < 3$, while $L_2(z)$ is analytic for $\mathrm{Re}(z) > 2$. We now show that $L_1(z)$ and $L_2(z)$ can be analytically continued as meromorphic functions in the complex z-plane.

Through an integration by parts in (B 6) we deduce

$$L_1(z) = \frac{p(t) - [\sin(\alpha/2)]^{z-1}}{(z-1)t^{z-1}}\bigg|_0^{\pi} + \int_0^{\pi}\{p(t) - [\sin(\alpha/2)]^{z-1}\}\frac{\mathrm{d}t}{t^z}, \quad (B\,7)$$

where

$$p(t) = \tfrac{1}{2}\{|\sin(t+\alpha/2)|^{z-1} + |\sin(t-\alpha/2)|^{z-1}\}. \quad (B\,8)$$

Since

$$p(t) - [\sin(\alpha/2)]^{z-1} = O(t^2) \quad (t \downarrow 0)$$

the first term on the right of (B 7) vanishes if $1 < \mathrm{Re}(z) < 3$, while the integral in (B 7) is convergent for $0 < \mathrm{Re}(z) < 3$. Thus we are led to the representation

$$L_1(z) = \int_0^{\pi}\{p(t) - [\sin(\alpha/2)]^{z-1}\}\frac{\mathrm{d}t}{t^z}, \quad (B\,9)$$

which provides the analytic continuation of $L_1(z)$ to the strip $0 < \mathrm{Re}(z) < 3$.

A similar integration by parts in the integral for $L_2(z)$ yields

$$L_2(z) = -\frac{[\sin(\alpha/2)]^{z-1}}{(z-1)\pi^{z-1}} + \int_{\pi}^{\infty}\frac{p(t)}{t^z}\,\mathrm{d}t. \quad (B\,10)$$

Here, the first term on the right is analytic except for a simple pole at $z = 1$ with residue -1, while the integral is convergent for $\mathrm{Re}(z) > 1$. Since $p(t)$ in (B 8) is periodic with period π, we may reduce the integral in (B 10) to

$$\int_{\pi}^{\infty}\frac{p(t)}{t^z}\,\mathrm{d}t = \sum_{k=0}^{\infty}\int_{(k+1)\pi}^{(k+2)\pi}\frac{p(t)}{t^z}\,\mathrm{d}t = \int_0^{\pi}p(t)\sum_{k=0}^{\infty}\frac{1}{[t+(k+1)\pi]^z}\,\mathrm{d}t$$

$$= \int_0^{\pi}p(t)\pi^{-z}\zeta(z, 1+t/\pi)\,\mathrm{d}t, \quad (B\,11)$$

valid for $\mathrm{Re}(z) > 1$; here, ζ with two arguments denotes the generalized zeta function, extensively discussed in Erdélyi *et al.* (1953, § 1.10). As a function of z, $\zeta(z, 1+t/\pi)$ is analytic in the whole z-plane, except for a simple pole at $z = 1$ with residue 1. Consequently, the final integral in (B 11) is analytic for $\mathrm{Re}(z) > 0$, except for a simple pole at $z = 1$ with residue equal to $\int_0^{\pi}\pi^{-1}\,\mathrm{d}t = 1$, because $p(t) = 1$ for $z = 1$. This singularity is precisely compensated by the first term on the right of (B 10). By inserting (B 11) into (B 10) we are led to the representation

$$L_2(z) = -\frac{[\sin(\alpha/2)]^{z-1}}{(z-1)\pi^{z-1}} + \int_0^{\pi}p(t)\pi^{-z}\zeta(z, 1+t/\pi)\,\mathrm{d}t, \quad (B\,12)$$

which is valid and analytic for $\mathrm{Re}(z) > 0$.

Next we combine the representations (B 9) and (B 12). For $0 < \mathrm{Re}(z) < 1$ we have in (B 9),

$$-\int_0^{\pi} [\sin(\alpha/2)]^{z-1} \frac{\mathrm{d}t}{t^z} = \frac{[\sin(\alpha/2)]^{z-1}}{(z-1)\pi^{z-1}}$$

which cancels with the first term on the right of (B 12). By use of the relation

$$\frac{1}{t^z} + \pi^{-z}\zeta(z, 1 + t/\pi) = \pi^{-z}\zeta(z, t/\pi)$$

and by inserting the value of $p(t)$ from (B 8), we obtain the following representation for $L(z)$ as the sum of $L_1(z)$ and $L_2(z)$:

$$L(z) = \frac{1}{2}\int_0^{\pi} \{|\sin(t + \alpha/2)|^{z-1} + |\sin(t - \alpha/2)|^{z-1}\}\, \pi^{-z}\zeta(z, t/\pi)\, \mathrm{d}t, \tag{B 13}$$

valid and analytic for $0 < \mathrm{Re}(z) < 1$.

We now employ Hurwitz's formula for $\zeta(z, t/\pi)$:

$$\zeta(z, t/\pi) = 2^z \pi^{z-1} \Gamma(1 - z) \sum_{n=1}^{\infty} n^{z-1} \sin(2nt + \pi z/2), \tag{B 14}$$

taken from Erdélyi *et al.* (1953, formula 1.10(6)). Inserting (B 14) into (B 13) and integrating term by term, leads to integrals of the form

$$I_n = \frac{1}{2}\int_0^{\pi} \{|\sin(t + \alpha/2)|^{z-1} + |\sin(t - \alpha/2)|^{z-1}\} \sin(2nt + \pi z/2)\, \mathrm{d}t, \tag{B 15}$$

where $n = 1, 2, 3, \ldots$. The integrand in (B 15) is periodic with period π, and the integration is over one period. By properly shifting the integration interval we deduce

$$\begin{aligned} I_n &= \frac{1}{2}\int_0^{\pi} (\sin t)^{z-1} [\sin(2nt - n\alpha + \pi z/2) + \sin(2nt + n\alpha + \pi z/2)]\, \mathrm{d}t \\ &= \cos(n\alpha)\cos(\pi z/2) \int_0^{\pi} (\sin t)^{z-1} \sin(2nt)\, \mathrm{d}t \\ &\quad + \cos(n\alpha)\sin(\pi z/2) \int_0^{\pi} (\sin t)^{z-1} \cos(2nt)\, \mathrm{d}t. \end{aligned} \tag{B 16}$$

The first of the latter two integrals vanishes because the integrand is odd with respect to $t = \pi/2$. The final integral is evaluated by means of Erdélyi *et al.* (1953, equation 1.5(29)), yielding

$$\int_0^{\pi} (\sin t)^{z-1} \cos(2nt)\, \mathrm{d}t = \frac{\pi}{2^{z-1}} \frac{\Gamma(z)(-1)^n}{\Gamma(1/2 + z/2 + n)\Gamma(1/2 + z/2 - n)}. \tag{B 17}$$

By collecting the previous results we find that the term-by-term integration in (B 13) leads to

$$\begin{aligned} L(z) &= 2\Gamma(z)\Gamma(1 - z)\sin(\pi z/2) \sum_{n=1}^{\infty} \frac{(-1)^n n^{z-1}\cos(n\alpha)}{\Gamma(1/2 + z/2 + n)\Gamma(1/2 + z/2 - n)} \\ &= \sum_{n=1}^{\infty} \frac{\Gamma(1/2 - z/2 + n)}{\Gamma(1/2 + z/2 + n)} \frac{\cos(n\alpha)}{n^{1-z}} \end{aligned} \tag{B 18}$$

by use of the reflection formula for the gamma function. Since

$$\frac{\Gamma(1/2-z/2+n)}{\Gamma(1/2+z/2+n)} = n^{-z}\left[1+O(n^{-2})\right] \quad (n\to\infty) \tag{B 19}$$

by Erdélyi *et al.* (1953, formula 1.18(4)), the series in (B 18) compares to $\sum_{n=1}^{\infty}\cos(n\alpha)/n$ and is convergent. The convergence can be improved by subtracting and adding

$$\sum_{n=1}^{\infty}\frac{\cos(n\alpha)}{n} = -\log[2\sin(\alpha/2)] \quad (0<\alpha<2\pi) \tag{B 20}$$

whereupon

$$L(z) = -\log[2\sin(\alpha/2)] + L^{*}(z), \tag{B 21}$$

$$L^{*}(z) = \sum_{n=1}^{\infty}\left\{\frac{\Gamma(1/2-z/2+n)}{\Gamma(1/2+z/2+n)}\frac{\cos(n\alpha)}{n^{1-z}} - \frac{\cos(n\alpha)}{n}\right\}. \tag{B 22}$$

In view of (B 19), the series (B 22) compares to $\sum_{n=1}^{\infty}\cos(n\alpha)/n^3$ and so is convergent for all z.

The representation (B 18), or (B 21)–(B 22), for $L(z)$ is valid, first for $0<\mathrm{Re}(z)<1$, and next for all complex z by analytic continuation. The terms in the final series in (B 18) have simple poles at $z=2k+1$, $k=1,2,3,\ldots$. Thus it follows that $L(z)$ is analytic in the whole z-plane, except for simple poles at $z=2k+1$, $k=1,2,3,\ldots$. We now return to the Mellin transforms $\mathscr{M}\{W_{1,2}(p)\}$ as given by (B 5). The factor $\Gamma(z/2)\Gamma(3/2-z/2)$ has simple poles at $z=-2k$, $k=0,1,2,\ldots$, and at $z=2k+1$, $k=1,2,3,\ldots$. Consequently, $\mathscr{M}\{W_1(p)+W_2(p)\}$ is analytic in the whole z-plane, except for simple poles at $z=-2k$, $k=0,1,2,\ldots$, and double poles at $z=2k+1$, $k=1,2,3,\ldots$. This leaves the strip $0<\mathrm{Re}(z)<3$ as the strip of analyticity of the Mellin transform $\mathscr{M}\{W_1(p)+W_2(p)\}=\mathscr{M}\{W(\alpha,p)-1/p\}$. By means of the Mellin inversion formula we arrive at the following representation of $W(\alpha,p)$ by a Mellin–Barnes integral:

$$W(\alpha,p) = \frac{1}{p} + \frac{1}{2\pi\mathrm{i}}\int_{c-\mathrm{i}\infty}^{c+\mathrm{i}\infty}\frac{\Gamma(z/2)\Gamma(3/2-z/2)}{2\Gamma(3/2)}L(z)p^{-z}\,\mathrm{d}z, \quad 0<c<3, \tag{B 23}$$

in which $L(z)$ is given by (B 18). By substitution of (B 21) for $L(z)$ and by use of the inverse of the transform (B 4) with $\nu=3/2$, we obtain the alternative representation

$$W(\alpha,p) = \frac{1}{p} - \log[2\sin(\alpha/2)]\,(p^2+1)^{-3/2} + \frac{1}{2\pi\mathrm{i}}\int_{c-\mathrm{i}\infty}^{c+\mathrm{i}\infty}\frac{\Gamma(z/2)\Gamma(3/2-z/2)}{2\Gamma(3/2)}L^{*}(z)p^{-z}\,\mathrm{d}z, \quad 0<c<3, \tag{B 24}$$

in which $L^{*}(z)$ is given by (B 22). These representations are used in § 3 to establish the asymptotics of $W(\alpha,p)$ both for small p and for large p.

Finally we consider the limit case $\alpha\downarrow 0$ of $W(\alpha,p)$. From (B 24) we infer

$$\lim_{\alpha\downarrow 0}[W(\alpha,p)+\log[2\sin(\alpha/2)](p^2+1)^{-3/2}] = \frac{1}{p} + \frac{1}{2\pi\mathrm{i}}\int_{c-\mathrm{i}\infty}^{c+\mathrm{i}\infty}\frac{\Gamma(z/2)\Gamma(3/2-z/2)}{2\Gamma(3/2)}P(z)p^{-z}\,\mathrm{d}z, \quad 0<c<3, \tag{B 25}$$

where

$$P(z) = \lim_{\alpha \downarrow 0} L^*(z) = \sum_{n=1}^{\infty} \left\{ \frac{\Gamma(1/2 - z/2 + n)}{\Gamma(1/2 + z/2 + n)} \frac{1}{n^{1-z}} - \frac{1}{n} \right\}, \tag{B 26}$$

in accordance with the notation $P(z)$ from BW (A 12). We want to express the limit (B 25) in terms of the integral $W(p)$, given by (2.1). To that end, we compare (B 25) to the Mellin–Barnes integral representation of $W(p)$, taken from BW (4.14), namely

$$W(p) = (p^2+1)^{-3/2} \log(p/2) + \frac{1}{2\pi \mathrm{i}} \int_{c-\mathrm{i}\infty}^{c+\mathrm{i}\infty} \frac{\Gamma(z/2)\Gamma(3/2 - z/2)}{2\Gamma(3/2)} R(z) p^{-z} \, \mathrm{d}z, \quad 1 < c < 3, \tag{B 27}$$

in which

$$\begin{aligned} R(z) &= -\frac{1}{z-1} + \psi(1/2 - z/2) + E + 2\log 2 + P(z) \\ &= P(z) + 2 + \psi(3/2 - z/2) - \psi(3/2) + \frac{1}{z-1}. \end{aligned} \tag{B 28}$$

The first line of (B 28) stems from BW (4.12); $E = 0.5772\ldots$ is Euler's constant, and $\psi(z) = \Gamma'(z)/\Gamma(z)$. The second line of (B 28) follows by use of some standard properties of the ψ-function. By combining (B 25) and (B 27) we deduce

$$\begin{aligned} &\lim_{\alpha \downarrow 0} \left[W(\alpha, p) + \log[2\sin(\alpha/2)] \, (p^2+1)^{-3/2} \right] \\ &= p^{-1} + W(p) - (p^2+1)^{-3/2} \log(p/2) - \frac{1}{2\pi \mathrm{i}} \int_{c-\mathrm{i}\infty}^{c+\mathrm{i}\infty} \frac{\Gamma(z/2)\Gamma(3/2 - z/2)}{2\Gamma(3/2)} \\ &\qquad \times \left[2 + \psi(3/2 - z/2) - \psi(3/2) + \frac{1}{z-1} \right] p^{-z} \, \mathrm{d}z, \end{aligned} \tag{B 29}$$

in which $1 < c < 3$. The latter integral is recognized as an inverse Mellin transform. By inversion of the transform (B 4) and of its derivative with respect to ν, at $\nu = 3/2$, we find

$$\begin{aligned} &\frac{1}{2\pi \mathrm{i}} \int_{c-\mathrm{i}\infty}^{c+\mathrm{i}\infty} \frac{\Gamma(z/2)\Gamma(3/2 - z/2)}{2\Gamma(3/2)} \left[2 + \psi(3/2 - z/2) - \psi(3/2) \right] p^{-z} \, \mathrm{d}z \\ &\qquad = (p^2+1)^{-3/2} [2 - \log(p^2+1)], \quad 0 < c < 3. \end{aligned} \tag{B 30}$$

The remaining integral in (B 29) is evaluated by shifting the integration path $\mathrm{Re}(z) = c$ over the pole at $z = 1$ to $\mathrm{Re}(z) = c'$, where $0 < c' < 1$. Thus we obtain

$$\begin{aligned} &\frac{1}{2\pi \mathrm{i}} \int_{c-\mathrm{i}\infty}^{c+\mathrm{i}\infty} \frac{\Gamma(z/2)\Gamma(3/2 - z/2)}{2\Gamma(3/2)} \frac{p^{-z}}{z-1} \, \mathrm{d}z \\ &= \frac{1}{p} - \frac{1}{2\pi \mathrm{i}} \int_{c'-\mathrm{i}\infty}^{c'+\mathrm{i}\infty} \frac{\Gamma(z/2)\Gamma(1/2 - z/2)}{2\Gamma(1/2)} p^{-z} \, \mathrm{d}z = p^{-1} - (p^2+1)^{-1/2}, \end{aligned} \tag{B 31}$$

based on inversion of the transform (B 4) with $\nu = 1/2$. Substitution of (B 30) and

(B 31) into (B 29) yields

$$\lim_{\alpha\downarrow 0}\left[W(\alpha,p)+\log[2\sin(\alpha/2)](p^2+1)^{-3/2}\right]$$

$$=W(p)+(p^2+1)^{-3/2}[p^2-1+\log 2+\log(p^2+1)-\log p], \quad \text{(B 32)}$$

which proves the limit result stated in (2.12).

REFERENCES

Bhagwat, M. J. & Leishman, J. G. 2000*a* Measurements of bound and wake circulation on a helicopter rotor. *J. Aircraft* **37**, 227–234.

Bhagwat, M. J. & Leishman, J. G. 2000*b* Stability analysis of helicopter rotor wakes in axial flight. *J. Am. Hel. Soc.* **45**, 165–178.

Bliss, D. B., Teske, M. E. & Quackenbush, T. R. 1987 A new methodology for free wake analysis using curved vortex elements. *NASA CR* 3958.

Boersma, J. & Wood, D. H. 1999 On the self-induced motion of a helical vortex. *J. Fluid Mech.* **384**, 263–280 (referred to herein as BW).

Boersma, J. & Yakubovich, S. B. 1998 Solution to problem $97-18^{*}$: the asymptotic sum of a Kapteyn series. *SIAM Rev.* **40**, 986–990.

Erdélyi, A., Magnus, W., Oberhettinger, F. & Tricomi, F. G. 1953 *Higher Transcendental Functions*, Vol. 1. McGraw-Hill.

Favier, D., Ettaouil, A. & Maresca, C. 1989 Numerical and experimental investigation of isolated propeller wakes in axial flight. *J. Aircraft* **26**, 837–846.

Favier, D. & Maresca, C. 1984 Etude du sillage 3D d'une helice aerienne. In *Aerodynamics and Acoustics of Propellers*, AGARD-CP-363, pp. 15-1–15-22.

Gupta, B. P. & Loewy, R. G. 1974 Theoretical analysis of the aerodynamic stability of multiple, interdigitated helical vortices. *AIAA J.* **12**, 1381–1387.

Hardin, J. C. 1982 The velocity field induced by a helical vortex filament. *Phys. Fluids* **25**, 1949–1952.

Kuibin, P. A. & Okulov, V. L. 1998 Self-induced motion and asymptotic expansion of the velocity field in the vicinity of a helical vortex filament. *Phys. Fluids* **10**, 607–614.

Leishman, J. G., Baker, A. & Coyne, A. 1996 Measurements of rotor tip vortices using three-component laser-Doppler velocimetry. *J. Am. Hel. Soc.* **41**, 342–353.

Lewin, L. 1981 *Polylogarithms and Associated Functions.* North Holland.

Moore, D. W. & Saffman, P. G. 1972 The motion of a vortex filament with axial flow. *Phil. Trans. R. Soc. Lond.* A **272**, 403–429.

Ricca, R. L. 1994 The effect of torsion on the motion of a helical vortex filament. *J. Fluid Mech.* **273**, 241–259.

Saffman, P. G. 1992 *Vortex Dynamics.* Cambridge University Press.

Spera, D. A. (Ed.) 1994 *Wind Turbine Technology: Fundamental Concepts of Wind Turbine Engineering*. ASME Press.

Wood, D. H. & Li, D. 2001 How accurately is a helical vortex represented by straight segments? *AIAA J.* (submitted).

Xu, G. & Sankar, L. N. 2000 Computational study of horizontal axis wind turbines. *J. Solar Energy Engng* **122**, 35–39.